At least 2 days after cortisol administration, individualized doses of docetaxel were diluted in 250 mL of 5% glucose or 0.9% saline and administered by 1-hour intravenous infusion at 9 AM to each patient. The doses of docetaxel in subsequent cycles of treatment were unchanged, and no prophylactic premedication to protect against docetaxel-related hypersensitivity reactions was administered in either of the treatment arms.

PK Study

Blood samples for PK studies were obtained from all of the patients during the initial treatment cycle. An indwelling cannula was inserted in the arm opposite that used for the drug infusion, and blood samples were collected into heparinized tubes. Blood samples were collected before the infusion; 30 minutes after the start of the infusion; at the end of the infusion; and 15, 30, and 60 minutes and 3, 5, 9, and 24 hours after the end of the infusion. All blood samples were centrifuged immediately at 4,000 rpm for 10 minutes, after which the plasma was removed and the samples were placed in polypropylene tubes, labeled, and stored at −20°C or colder until analysis.

PK parameters were estimated by the nonlinear least squares regression analysis method (WinNonlin, Version 1.5; Bellkey Science Inc, Chiba, Japan) with a weighting factor of 1 per year.[2] Individual plasma concentration-time data were fitted to two- and three-compartment PK models using a zero-order infusion input and first-order elimination. The model was chosen on the basis of Akaike's information criteria.[31] The peak plasma concentration (C_{max}) was generated directly from the experimental data. AUC was extrapolated to infinity and determined based on the best-fitted curve; this measurement was then used to calculate the absolute CL (L/h), defined as the ratio of the delivered dosage (in milligrams) and AUC.

To assess PD effect of docetaxel, the percentage decrease in ANC was calculated according to the following formula: % decrease in ANC = (pretreatment ANC − nadir ANC)/(pretreatment ANC) × 100.

Measurements

The concentration of urinary 6-β-OHF was measured by reversed phase high-performance liquid chromatography with UV absorbance detection according to previously published methods.[30,32,33]

Docetaxel concentrations in plasma were also measured by solid-phase extraction and reversed phase high-performance liquid chromatography with UV detection according to the previously published method.[30,34] The detection limit corresponded to a concentration of 10 ng/mL.

Statistical Analysis

Fisher's exact test or χ^2 test was used to compare categoric data, and Student's t test was used for continuous variables. The strength of the relationship between the estimated docetaxel CL and the observed docetaxel CL was assessed by least squares linear regression analysis. The interpatient variability of AUC for each arm was evaluated by determining the SD and was compared by F test. Biases, or the mean AUC value in each arm minus the target AUC (2.66 mg/L · h), were also compared between the arms by Student's t test.

A two-sided P value of ≤ .05 or less was considered to indicate statistical significance. All statistical analyses were performed using SAS software version 8.02 (SAS Institute, Cary, NC).

RESULTS

Patient Characteristics

Between October 1999 and May 2001, 59 patients were enrolled onto the study and randomly assigned to either the BSA-based arm (n = 30) or the individualized arm (n = 29). All 59 patients were assessable for PK and PD analyses. The pretreatment characteristics of the 59 patients are listed in Table 1. The baseline characteristics were well balanced between the arms except for three laboratory parameters: ALB, AAG, and ALP. These three parameters were not included in the eligibility criteria. The majority of patients (95%) had a performance status of 0 or 1. Twenty (67%) and 16 (55%) patients had been treated with platinum-based chemotherapy in the BSA-based arm and individualized arm, respectively. Only two patients in the individualized arm had liver metastasis, and most of the patients had good hepatic functions.

Individualized Dosing of Docetaxel

In the individualized arm, the total amount of 24-hour urinary 6-β-OHF after cortisol administration (total 6-β-OHF) was 9,179.6 ± 3,057.7 μg/d (mean ± SD), which was similar to the result of our previous study.[30] The estimated docetaxel CL was 21.9 ± 3.5 L/h/m^2 (mean ± SD), and individualized dose of docetaxel ranged from 37.4 to 76.4 mg/m^2 (mean, 58.1 mg/m^2; Fig 1).

PK

Docetaxel PK data were obtained from all 59 patients during the first cycle of therapy, and PK parameters are listed in Table 2. Drug levels declined rapidly after infusion and could be determined to a maximum of 25 hours. The concentration of docetaxel in plasma was fitted to a biexponential equation, which was consistent with previous reports.[30,35-38] The mean alpha and beta half-lives were 9.2 minutes and 5.0 hours in the BSA-based arm and 9.2 minutes and 7.4 hours in the individualized arm, respectively.

In the BSA-based arm, docetaxel CL was 22.6 ± 3.4 L/h/m^2 (mean ± SD), and AUC averaged 2.71 mg/L · h (range, 2.02 to 3.40 mg/L · h). In the individualized arm, docetaxel CL was 22.1 ± 3.4 L/h/m^2, and AUC averaged 2.64 mg/L · h (range, 2.15 to 3.07 mg/L · h). The least squares linear regression analysis showed that the observed docetaxel CL was well estimated in the individualized arm (r^2 = 0.821; Fig 2).

The SDs of AUC in the BSA-based arm and in the individualized arm were 0.40 and 0.22, respectively, and the ratio of SD in the individualized arm to that in the BSA-based arm was 0.538 (95% CI, 0.369 to 0.782). The biases from the target AUC in the BSA-based arm and in the individualized arm were 0.047 (95% CI, −0.104 to 0.198) and −0.019 (95% CI, −0.102 to 0.064), respectively, with no significant difference. The interpatient variability of

Table 1. Patient Characteristics

Characteristic	BSA-Based Arm No. of Patients	%	Individualized Arm No. of Patients	%	P
Enrolled	30		29		
Eligible	30	100	29	100	
Age, years					.62
Median	61		62		
Range	52-73		45-73		
Sex					
Male	25	83	19	66	.14
Female	5	17	10	34	
ECOG PS					
0	7	23	1	3	.08
1	22	73	26	90	
2	1	3	2	7	
Prior treatment					
None	4	13	4	14	.99
Surgery	11	37	9	31	.65
Radiotherapy	13	43	10	34	.49
Chemotherapy	21	70	18	62	.52
Platinum-based regimens	20	67	16	55	.37
Site of disease					
Lung	23	77	28	97	.10
Liver	0	0	2	7	.24
Pleura	8	27	12	41	.23
Bone	7	23	9	31	.71
Extrathoracic lymph nodes	0	33	10	34	.93
Laboratory parameters					
ALB, g/L					.02
Median	38		35		
Range	26-45		24-44		
AAG, g/L					.04
Median	1.00		1.25		
Range	0.28-2.15		0.64-2.54		
AST, U/L					.67
Median	21		22		
Range	10-40		7-41		
ALT, U/L					.88
Median	18		18		
Range	6-54		4-45		
ALP, U/L					.03
Median	249		324		
Range	129-540		185-986		

Abbreviations: ECOG, Eastern Cooperative Oncology Group; PS, performance status, ALB, serum albumin; AAG, alpha-1-acid glycoprotein; ALP, serum alkaline phosphatase.

AUC was significantly smaller in the individualized arm than in the BSA-based arm ($P < .01$; Fig 3).

PD

In both arms, neutropenia was the predominant toxicity related to docetaxel treatment, and 28 of 30 (93%) patients in the BSA-based arm and 25 of 29 (86%) patients in the individualized arm had grade 3 or 4 neutropenia.

Table 2. Docetaxel PK Parameters

Parameters	BSA-Based Arm (n = 30)	Individualized Arm (n = 29)
C_{max}, μg/mL	0.36-2.70	0.99-2.41
$t_{1/2}$ alpha*, minutes	9.2 ± 3.3	9.2 ± 2.7
$t_{1/2}$ beta*, hours	5.0 ± 4.8	7.4 ± 11.7
CL* L/h	37.6 ± 6.3	34.8 ± 7.1
CL* L/h/m²	22.6 ± 3.4	22.1 ± 3.4
AUC		
Mean mg/L · h	2.71	2.64
Range mg/L · h	2.02-3.40	2.15-3.07
Median	2.65	2.66
SD	0.40	0.22

Abbreviations: PK, pharmacokinetic; BSA, body-surface area; CL, clearance; AUC, area under concentration-time curve; SD, standard deviation.
*Data represent mean ± SD.

Nonhematologic toxicities, such as gastrointestinal and hepatic toxicities (ie, hyperbilirubinemia, aminotransferase elevations), were mild in both arms.

PD effects shown as the percentage decrease in ANC are listed in Table 3. The percentage decrease in ANC for the BSA-based arm and individualized arm were 87.1% (range, 59.0 to 97.7%; SD, 8.7) and 87.5% (range, 78.0 to 97.2%; SD, 6.1), respectively, suggesting that the interpatient variability in the percentage decrease in ANC was slightly smaller in the individualized arm than in the BSA-based arm (Fig 4). The response rates between the two arms were similar; five of 30 (16.7%) and four of 29 (13.8%) patients

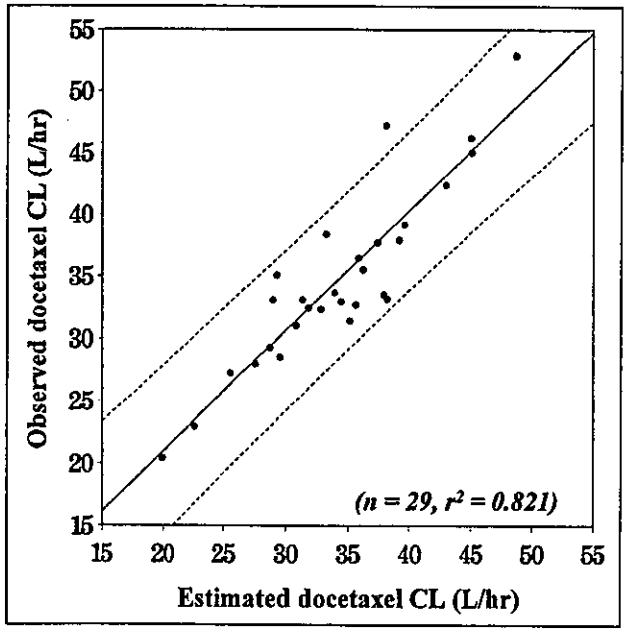

Fig 2. Correlation between the estimated and observed docetaxel clearance (CL) in the individualized arm (n = 29). (—) Linear regression line (r^2 = 0.821); (– – –) 95% CIs for individual estimates.

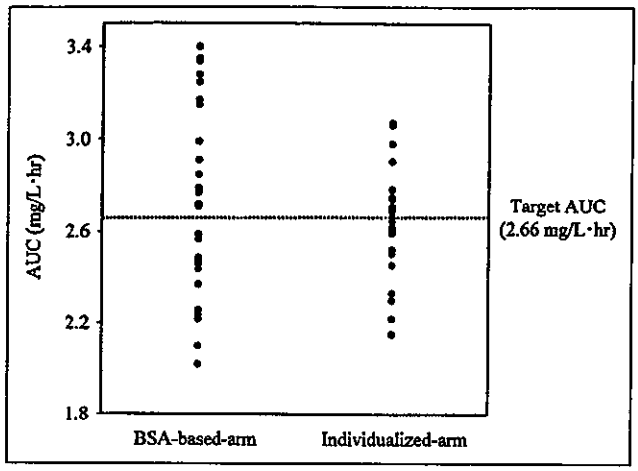

Fig 3. Comparison of area under the concentration-time curve (AUC) variability between the arms ($P < .01$; F test). BSA, body-surface area.

achieved a partial response in the BSA-based arm and individualized arm, respectively.

DISCUSSION

In oncology practice, the prescribed dose of most anticancer drugs is currently calculated from BSA of individual patients to reduce the interpatient variability of drug exposure. However, PK parameters, such as CL of many anticancer drugs, are not related to BSA.[2,39-43] Although PK parameters of docetaxel are correlated with BSA, individualized dosing based on individual metabolic capacities could further decrease the interpatient variability.[43]

CYP3A4 plays an important role in the metabolism of many drugs, including anticancer agents such as docetaxel, paclitaxel, vinorelbine, and gefitinib. This enzyme exhibits a large interpatient variability in metabolic activity, accounting for the large interpatient PK and PD variability. We have developed a novel method of estimating the interpatient variability of CYP3A4 activity by urinary metabolite of exogenous cortisol. That is, the total amount of 24-hour urinary 6-β-OHF after cortisol administration was highly correlated with docetaxel CL. We conducted a prospective randomized PK and PD study of docetaxel to evaluate whether the application of our method to individualized dosing could decrease PK and PD variability compared with BSA-based dosing.

Table 3. Percentage Decrease in ANC

Parameters	BSA-Based Arm (n = 30)	Individualized Arm (n = 29)
Percentage decrease in ANC, %		
Mean	87.1	87.4
Range	59.0-97.7	78.0-97.2
Median	89.7	88.4
SD	8.7	8.1

Abbreviations: ANC, absolute neutrophil count; BSA, body-surface area; SD, standard deviation.

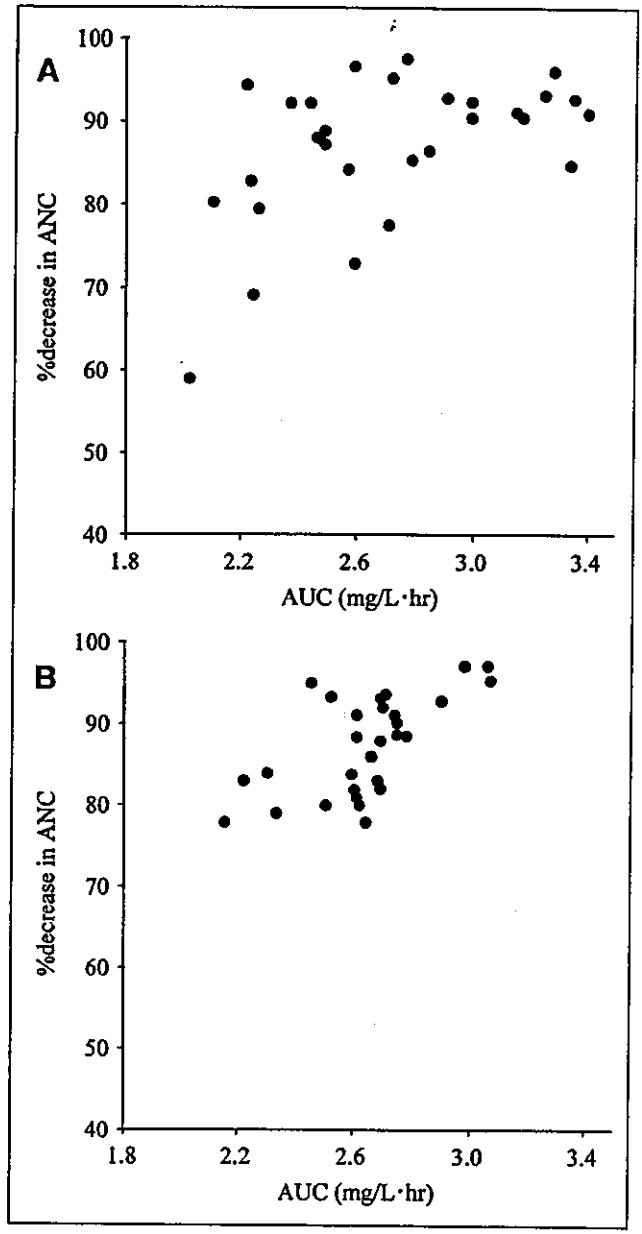

Fig 4. Correlation between area under the concentration-time curve (AUC) and percentage decrease in absolute neutrophil count (ANC) in each arm. (A) body-surface area–based arm; (B) individualized arm.

The study by Hirth et al[28] showed a good correlation between the result of the erythromycin breath test and docetaxel CL, and the study by Goh et al[29] showed a good correlation between the midazolam CL and docetaxel CL. In our study, we prospectively validated the correlation between docetaxel CL and our previously published method using the total amount of urinary 6-β-OHF after

cortisol administration in the individualized arm. As shown in Fig 2, the observed docetaxel CL was well estimated, and the equation for the estimation of docetaxel CL developed in our previous study was found to be reliable and reproducible. The target AUC in the individualized arm was set at 2.66 mg/L · h. This value was the mean value from our previous study, in which 29 patients were treated with 60 mg/m^2 of docetaxel. Individualized doses of docetaxel ranged from 37.4 to 76.4 mg/m^2 and were lower than expected.

The SD of AUC in the individualized arm was about 46.2% smaller than that in the BSA-based arm, a significant difference; this result seems to indicate that the application of our method to individualized dosing can reduce the interpatient PK variability. Assuming that the variability of AUC could be decreased 46.2% by individualized dosing applying our method, overtreatment could be avoided in 14.5% of BSA-dosed patients by using individualized dosing (Fig 5, area A), and undertreatment could be avoided in another 14.5% of these patients (Fig 5, area B). We considered that neutropenia could be decreased with patients in area A by individualized dosing. However, it is unknown whether the therapeutic effect of docetaxel could be improved in the patients in area B by individualized dosing because no significant positive correlation has been found between docetaxel AUC and antitumor response in patients with non–small-cell lung cancer.[43] In this study, seven of 30

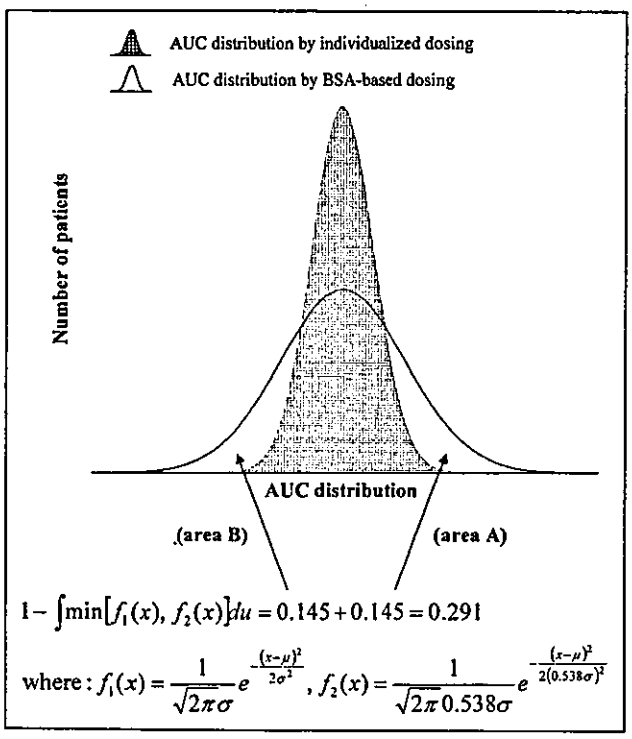

Fig 5. Simulated comparison of area under the concentration-time curve (AUC) distribution between body-surface area (BSA) –based dosing and individualized dosing when the variability of AUC is decreased 46.2% by individualized dosing applied using our method.

(23.3%) and two of 30 (6.7%) patients in the BSA-based arm were included in area A and B, respectively (Figs 3 and 5).

As shown in Figure 4, the percentage decrease in ANC was well correlated with AUC in both arms, which was similar to previous reports.[37,43] It was also indicated that the interpatient variability in the percentage decrease in ANC was slightly smaller in the individualized arm than in the BSA-based arm; however, this difference was not significant. The response rates between the two arms were similar. Although the interpatient PK variability could be decreased by individualized dosing in accordance with our method, the interpatient PD variability such as toxicity and the antitumor response could not be decreased. Several reasons could be considered.

With regard to toxicity, the pretreatment characteristics of the patients in this study were highly variable. More than half of the patients in each arm had previously received platinum-based chemotherapy, and more than 30% had received radiotherapy. The laboratory parameters (ie, ALB, AAG, and ALP) were not balanced across the arms, although they were not included in the eligibility criteria (Table 1). These variable pretreatment characteristics and unbalanced laboratory parameters may have influenced the frequency and severity of the hematologic toxicity as well as the pharmacokinetic profiles. The antitumor effect may have been influenced by the intrinsic sensitivity of tumors, the variable pretreatment characteristics, and the imbalance in laboratory parameters. Non–small-cell lung cancer is a chemotherapy-resistant tumor. The response rate for docetaxel ranges from 18% to 38%,[5] and no significant positive correlation between docetaxel AUC and antitumor response has been found. We considered it quite difficult to control the interpatient PD variability by controlling the interpatient PK variability alone. Although we did not observe any outliers in either arm, such as the two outliers with severe toxicity observed in the study by Hirth et al,[28] our method may be more useful for identifying such outliers. If we had not excluded patients with more abnormal liver function or a history of liver disease by the strict eligibility criteria, the results with the two dosing regimens may have been more different, and the interpatient PD variability, such as the percentage decrease in ANC, may have been smaller in the individualized arm than in the BSA-based arm. Furthermore, the primary end point of this study was PK variability, evaluated by the SD of AUC in both arms, and the sample size was significantly underpowered to evaluate whether the application of our method to individualized dosing could decrease PD variability compared with BSA-based dosing.

For the genotypes of CYP3A4, several genetic polymorphisms have been reported (http://www.imm.ki.se/CYPalleles/); however, a clear relationship between genetic polymorphisms and the enzyme activity of CYP3A4 has not been reported. Our phenotype-based

individualized dosing using the total amount of urinary 6-β-OHF after cortisol administration produced good results. However, this method is somewhat complicated, and a simpler method would be of great use. We analyzed the expression of CYP3A4 mRNA in the peripheral-blood mononuclear cells of the 29 patients in the individualized arm. No correlation was observed between the expression level of CYP3A4 mRNA and docetaxel CL or the total amount of urinary 6-β-OHF after cortisol administration (data not shown).

In conclusion, the individualized dosing of docetaxel using the total amount of urinary 6-β-OHF after cortisol administration is useful for decreasing the interpatient PK variability compared with the conventional BSA-based method of dosing. This method may be useful for individualized chemotherapy.

Authors' Disclosures of Potential Conflicts of Interest

The authors indicated no potential conflicts of interest.

REFERENCES

1. Sawyer M, Ratain MJ: Body surface area as a determinant of pharmacokinetics and drug dosing. Invest New Drugs 19:171-177, 2001
2. Gurney H: Dose calculation of anticancer drugs: A review of the current practice and introduction of an alternative. J Clin Oncol 14: 2590-2611, 1996
3. Ratain MJ: Body-surface area as a basis for dosing of anticancer agents: Science, myth, or habit? J Clin Oncol 16:2297-2298, 1998
4. Ringel I, Horwitz SB: Studies with RP 56976 (Taxotere): A semisynthetic analogue of taxol. J Natl Cancer Inst 83:288-291, 1991
5. Cortes JE, Pazdur R: Docetaxel. J Clin Oncol 13:2643-2655, 1995
6. Fossella FV, Lee JS, Murphy WK, et al: Phase II study of docetaxel for recurrent or metastatic non-small-cell lung cancer. J Clin Oncol 12:1238-1244, 1994
7. Fossella FV, Lee JS, Shin DM, et al: Phase II study of docetaxel for advanced or metastatic platinum-refractory non-small-cell lung cancer. J Clin Oncol 13:645-651, 1995
8. Gandara DR, Vokes E, Green M, et al: Activity of docetaxel in platinum-treated non-small-cell lung cancer: Results of a phase II multicenter trial. J Clin Oncol 18:131-135, 2000
9. Kunitoh H, Watanabe K, Onoshi T, et al: Phase II trial of docetaxel in previously untreated advanced non-small-cell lung cancer: A Japanese cooperative study. J Clin Oncol 14:1649-1655, 1996
10. Fossella FV, DeVore R, Kerr RN, et al: Randomized phase III trial of docetaxel versus vinorelbine or ifosfamide in patients with advanced non-small-cell lung cancer previously treated with platinum-containing chemotherapy regimens: The TAX 320 Non-Small Cell Lung Cancer Study Group. J Clin Oncol 18:2354-2362, 2000
11. Shepherd FA, Dancey J, Ramlau R, et al: Prospective randomized trial of docetaxel versus best supportive care in patients with non–small-cell lung cancer previously treated with platinum-based chemotherapy. J Clin Oncol 18:2095-2103, 2000
12. Hudis CA, Seidman AD, Crown JP, et al: Phase II and pharmacologic study of docetaxel as initial chemotherapy for metastatic breast cancer. J Clin Oncol 14:58-65, 1996
13. Trudeau ME, Eisenhauer EA, Higgins BP, et al: Docetaxel in patients with metastatic breast cancer: A phase II study of the National Cancer Institute of Canada-Clinical Trials Group. J Clin Oncol 14:422-428, 1996
14. Chan S, Friedrichs K, Noel D, et al: Prospective randomized trial of docetaxel versus doxorubicin in patients with metastatic breast cancer: The 303 Study Group. J Clin Oncol 17:2341-2354, 1999
15. Marre F, Sanderink GJ, de Sousa G, et al: Hepatic biotransformation of docetaxel (Taxotere) *in vitro*: Involvement of the CYP3A subfamily in humans. Cancer Res 56:1296-1302, 1996
16. Nelson DR, Koymans L, Kamataki T, et al: P450 superfamily: Update on new sequences, gene mapping, accession numbers and nomenclature. Pharmacogenetics 6:1-42, 1996
17. Lin JH, Lu AYH: Inhibition and induction of cytochrome P450 and the clinical implications. Clin Pharmacokinet 35:361-390, 1998
18. Parkinson A: An overview of current cytochrome P450 technology for assessing the safety and efficacy of new materials. Toxicol Pathol 24:45-57, 1996
19. Shimada T, Yamazaki H, Mimura M, et al: Interindividual variations in human liver cytochrome P-450 enzymes involved in the oxidation of drugs, carcinogens and toxic chemicals: Studies with liver microsomes of 30 Japanese and 30 Caucasians. J Pharmacol Exp Ther 270:414-423, 1994
20. Guengerich FP: Characterization of human microsomal cytochrome P450 enzymes. Annu Rev Pharmacol Toxicol 29:241-264, 1989
21. Guengerich FP, Turvy CG: Comparison of levels of human microsomal cytochrome P450 enzymes and epoxide hydrolase in normal and disease status using immunochemical analysis of surgical samples. J Pharmacol Exp Ther 256: 1189-1194, 1991
22. Hunt CM, Westerkam WR, Stave GM: Effects of age and gender on the activity of human hepatic CYP3A. Biochem Pharmacol 44: 275-283, 1992
23. Watkins PB, Turgeon DK, Saenger P, et al: Comparison of urinary 6-beta-cortisol and the erythromycin breath test as measures of hepatic P450IIIA (CYP3A) activity. Clin Pharmacol Ther 52:265-273, 1992
24. Kinirons MT, O'Shea D, Downing TE, et al: Absence of correlations among three putative *in vivo* probes of human cytochrome P4503A activity in young healthy men. Clin Pharmacol Ther 54:621-629, 1993
25. Hunt CM, Watkins PB, Saenger P, et al: Heterogeneity of CYP3A isoforms metabolizing erythromycin and cortisol. Clin Pharmacol Ther 51:18-23, 1992
26. Thummel KE, Shen DD, Podoll TD, et al: Use of midazolam as a human cytochrome P450 3A probe: II. Characterization of inter- and intra-individual hepatic CYP3A variability after liver transplantation. J Pharmacol Exp Ther 271:557-566, 1994
27. Thummel KE, Shen DD, Podoll TD, et al: Use of midazolam as a human cytochrome P450 3A probe: I. In vitro-in vivo correlations in liver transplant patients. J Pharmacol Exp Ther 271: 549-556, 1994
28. Hirth J, Watkins PB, Strawderman M, et al: The effect of an individual's cytochrome CYP3A4 activity on docetaxel clearance. Clin Cancer Res 6:1255-1258, 2000
29. Goh BC, Lee SC, Wang LZ, et al: Explaining interindividual variability of docetaxel pharmacokinetics and pharmacodynamics in Asians through phenotyping and genotyping strategies. J Clin Oncol 20:3683-3690, 2002
30. Yamamoto N, Tamura T, Kamiya Y, et al: Correlation between docetaxel clearance and estimated cytochrome P450 activity by urinary metabolite of exogenous cortisol. J Clin Oncol 18:2301-2308, 2000
31. Yamaoka K, Nakagawa T, Uno T: Application of Akaike's information criterion (AIC) in the evaluation of linear pharmacokinetic equations. J Pharmacokinet Biopharm 6:165-175, 1978
32. Nakamura J, Yakata M: Determination of urinary cortisol and 6 beta-hydroxycortisol by high performance liquid chromatography. Clin Chim Acta 149:215-224, 1985
33. Lykkesfeldt J, Loft S, Poulsen HE: Simultaneous determination of urinary free cortisol and 6 beta-hydroxycortisol by high-performance liquid chromatography to measure human CYP3A activity. J Chromatogr B Biomed Appl 660:23-29, 1994
34. Vergniol JC, Bruno R, Montay G, et al: Determination of Taxotere in human plasma by a semi-automated high-performance liquid chromatographic method. J Chromatogr 582:273-278, 1992
35. Taguchi T, Furue H, Niitani H, et al: Phase I clinical trial of RP 56976 (docetaxel) a new anticancer drug. Gan To Kagaku Ryoho 21:1997-2005, 1994
36. Burris H, Irvin R, Kuhn J, et al: Phase I clinical trial of Taxotere administered as either a 2-hour or 6-hour intravenous infusion. J Clin Oncol 11:950-958, 1993
37. Extra JM, Rousseau F, Bruno R, et al: Phase I and pharmacokinetic study of Taxotere (RP 56976; NSC 628503) given as a short

intravenous infusion. Cancer Res 53:1037-1042, 1993

38. Pazdur R, Newman RA, Newman BM, et al: Phase I trial of Taxotere: Five-day schedule. J Natl Cancer Inst 84:1781-1788, 1992

39. Mathijssen RHJ, Verweij J, de Jonge MJ, et al: Impact of body-size measures on irinotecan clearance: Alternative dosing recommendations. J Clin Oncol 20:81-87, 2002

40. De Jongh FE, Verweij J, Loos WJ, et al: Body-surface area-based dosing does not increase accuracy of predicting cisplatin exposure. J Clin Oncol 19:3733-3739, 2001

41. Gurney HP, Ackland S, Gebski V, et al: Factors affecting epirubicin pharmacokinetics and toxicity: Evidence against using body-surface area for dose calculation. J Clin Oncol 16:2299-2304, 1998

42. Loos WJ, Gelderblom H, Sparreboom A, et al: Inter- and intrapatient variability in oral topotecan pharmacokinetics: Implications for body-surface area dosage regimens. Clin Cancer Res 6:2685-2689, 2000

43. Bruno R, Hille D, Riva A, et al: Population pharmacokinetics/pharmacodynamics of docetaxel in phase II studies in patients with cancer. J Clin Oncol 16:187-196, 1998

Available online at www.sciencedirect.com
SCIENCE DIRECT®
Biochemical and Biophysical Research Communications 313 (2004) 931–937
BBRC
www.elsevier.com/locate/ybbrc

Highly specific marker genes for detecting minimal gastric cancer cells in cytology negative peritoneal washings

Kazuhiko Mori,[a,f] Kazuhiko Aoyagi,[a] Tetsuya Ueda,[f] Inaho Danjoh,[b] Yasuhiro Tsubosa,[g] Kazuyoshi Yanagihara,[c] Yoshihiro Matsuno,[d] Mitsuru Sasako,[e] Hiromi Sakamoto,[a] Ken-ichi Mafune,[f] Michio Kaminishi,[f] Teruhiko Yoshida,[a,b] Masaaki Terada,[a] and Hiroki Sasaki[a,*]

[a] *Genetics Division, National Cancer Center Research Institute, Tokyo 104-0045, Japan*
[b] *Center of Medical Genomics, National Cancer Center Research Institute, Tokyo, Japan*
[c] *Central Animal Laboratory, National Cancer Center Research Institute, Tokyo, Japan*
[d] *Clinical Laboratory, National Cancer Center Hospital, Tokyo, Japan*
[e] *Surgical Oncology Department, National Cancer Center Hospital, Tokyo, Japan*
[f] *Department of Gastrointestinal Surgery, University of Tokyo Graduate School of Medicine, Tokyo, Japan*
[g] *Division of Esophageal Surgery, Shizuoka Cancer Center Hospital, Shizuoka, Japan*

Received 21 November 2003

Abstract

Peritoneal wash cytology plays a pivotal role in the decision for gastric cancer treatment because advanced gastric cancer often turns out incurable with peritoneal metastasis. Molecular detection of minimal cancer cells from peritoneal washings may overcome the sensitivity boundary of conventional cytology and contribute to the prediction of the disease outcome. To select marker candidates out of ten thousands of genes, we performed microarray analyses in 12 gastric cell lines and 8 peritoneal washings of early stage cases. With 40 candidates selected by the above expression profiling, RT-PCR in 16 representative peritoneal wash samples was performed to identify genes specific to cytology positive samples. The finally selected five genes, *CK20*, *FABP1*, *MUC2*, *TFF1*, and *TFF2*, were then evaluated for their utility as a marker for minimal residual disease in 99 peritoneal wash samples. Nested RT-PCR using the five genes showed positive results highly specific to incurable cases (91–100%). With a high specificity, the combination of these five genes succeeded in identifying 6 out of 20 (30%) additional patients with all types of early recurrence that could not be predicted by the conventional method. The six newly identified recurrences included four non-peritoneal ones, showing that RT-PCR using the five genes without a real-time quantitative PCR technique contributes to the detection of minimal residual disease.

Keywords: Molecular marker; Gastric cancer; Peritoneal washing; Minimal residual disease

In the detection of cancer cells from various kinds of samples, many researchers aim for the development of new techniques that overcome the detection limit of conventional immunostaining and cytology. Methylation-specific PCR in ductal lavage fluid for breast cancer [1] and digital protein truncation assay in a stool sample for colorectal cancer [2] are good examples. mRNAs are also a good target for cancer cell detection. To date, many reports on mRNA detection of cancer cells have been published but the essential task, the selection of candidate genes, is knowledge-dependent in most of those previous studies.

As for gastric cancer, mRNAs from peritoneal washings or lymph nodes are used to demonstrate minimal residual disease in investigational studies [3–5]. For advanced gastric cancer, peritoneal cytology plays the pivotal role in the decision for treatment strategy because peritoneal metastasis is the commonest mode of recurrence [6] and discourages radical surgery. However,

* Corresponding author. Fax: +81-3-3541-2685.
E-mail address: hksasaki@gan2.res.ncc.go.jp (H. Sasaki).

0006-291X/$ - see front matter © 2003 Elsevier Inc. All rights reserved.
doi:10.1016/j.bbrc.2003.12.025

not a few gastric cancer patients with negative cytology develop peritoneal metastasis as a result of the sensitivity boundary of cytology. mRNA detection of cancer cells from peritoneal washings may provide us with a more sensitive way, and efforts are being made to establish detection techniques. Carcinoembryonic antigen (*CEA*) is a well-known tumor marker and has been used to detect a very small number of adenocarcinoma cells in the blood, peritoneal wash or other body fluids [3,7,8]. The expression of *CEA* mRNA, however, is not specific to cancer cells and often produces false positive results [9]. Other more specific genes are awaited for more accurate diagnosis.

Therefore, we conducted a gene screening using microarray in a search for a molecular marker of gastric cancer cells in the peritoneal cavity.

Materials and methods

Peritoneal wash samples and patient profiles. One hundred and eight peritoneal wash samples and 46 gastric cancer tissues were collected from 108 out of 235 consecutive gastric cancer patients who gave written informed consent and whose surgery was performed from August 1999 to March 2000 at the National Cancer Center Hospital, Japan. Patients with clinically advanced disease were always candidates for peritoneal wash cytology. One hundred milliliters of the peritoneal washings collected during surgery was halved for cytology and RNA extraction. If massive ascites was present, the ascites was sampled instead. From 21 patients with early disease, the entire wash samples were used only for RNA extraction. Nine patients were excluded because of loss of follow-up, recent history of another intra-abdominal cancer, or metachronous peritoneal metastasis after positive surgical margin. All disease-free patients were followed up at least 2 years. Patients were evaluated for recurrence through consultation visit, measurement of serum CEA, and CA19-9 at 3-month intervals, and clinical imaging once a year including chest X-ray, abdominal ultrasonography, and computerized tomography scanning. In cases where recurrence was suspected, these routine imaging techniques and barium contrast enema were used for the establishment of diagnosis. Patients without evident incurable factors had no adjuvant therapies as long as no disease recurrence was confirmed except for a small number of participants in a clinical trial.

Cell lines. As a positive control for the first gene screening with microarray, we used gastric cancer cell lines instead of positive cytology samples because the cellular population of cancer cells on cytology positive slides was below 10% in most cases. Eight cell lines derived from diffuse-type gastric cancer, HSC39, HSC43, HSC44, HCS58, HSC59, HSC60, OCUM2M, and KATO III, and four cell lines from intestinal-type gastric cancer, HSC57, MKN7, MKN28, and MKN74,

Table 1
Primer sequences

Gene	Outer forward primers Outer reverse primers	Inner forward primers Inner reverse primers
CK20	5′-CAGACACACGGTGAACTATGG-3′ 5′-GATCAGCTTCCACTGTTAGACG-3′	5′-GGGACCTGTTTGTTGGCAATG-3′ 5′-ATTTGCAGGACACACCGAGCAT-3′
FABP1	5′-GAGCCAGGAAAACTTTGAAGC-3′ 5′-CAATGTCACCCAATGTCATGG-3′	5′-TCATGAAGGCAATCGGTCTG-3′ 5′-GTGATTATGTCGCCGTTGAGT-3′
MUC2	5′-CCGGGGAGTGCTGTAAGAAG-3′ 5′-GCTCTCGATGTGGGTGTAGG-3′	5′-GACAACCAGCACGTCATCCT-3′ 5′-CTCCTCTTTGCAGCAGGAGC-3′
TFF1	5′-CAGACAGAGACGTGTACAGT-3′ 5′-AAGTCAGAGCAGTCAATCTGT-3′	5′-CCCGTGAAAGACAGAATTGTG-3′ 5′-CCGAGCT-CTGGGACTAATCA-3′
TFF2	5′-CTGGAATCACCAGTGACCAGT-3′ 5′-GGCACTTCAAAGATGAAGTTG-3′	5′-ATGGATGCTGTTTCGACTCC-3′ 5′-GGCACTTCAAAGATGAAGTTG-3′
MASPIN	5′-CTCACAATAGCCGATATCAGA-3′ 5′-AATCTCAGAACAAGAAGAACCT-3′	
GW112	5′-CTCCTCGAGGGACCAAATCT-3′ 5′-CACTTTGTCACTGCCATCAG-3′	
PRSS4	5′-CTGGGCACAGTTGCTGTCCC-3′ 5′-GGCCACCAGAGTCACGCTGG-3′	
MDK	5′-CCTGCAACTGGAAGAAGGAG-3′ 5′-GGAGGCTCAAGCTTCCCAGA-3′	
SOX9	5′-GGTTGTTGGAGCTTTCCTCA-3′ 5′-AGCAATCCTCAAACTCTCTAG-3′	
CDX1	5′-ACTGAACGGCAGGTGAAGAT-3′ 5′-AGGGTGGATAGGTGACTGTC-3′	
CEA	5′-TCTGGAACTTCTCCTGGTCTCTCAGCTGG-3′ 5′-TGTAGCTGTTGCAAATGCTTTAAGGAAGAAGC-3′	5′-GGGCCACTGTCGGCATCATGATTGG-3′ 5′-TGTAGCTGTTGCAAATGCTTTAAGGAAGAAGC-3′
β-Actin	CACTGTGTTGGCGTACAGGT-3′ TCATCACCATTGGCAATGAG-3′	

were maintained in RPMI1640 supplemented with 10% fetal calf serum, 0.15% sodium bicarbonate, 2 mM L-glutamine, and penicillin–streptomycin. Cells were harvested only for RNA extraction.

RNA extraction. All the specimens and the pellets of the peritoneal washings were frozen immediately in liquid nitrogen and stored at −80 °C until use. For total RNA isolation, ISOGEN kit (Nippon Gene, Toyama, Japan) was used.

Gene screening strategy using microarray. We performed microarray analyses of gene expression in the clinical materials and gastric cell lines to screen out marker genes capable of detecting gastric cancer cells in the peritoneal washings using Affimetrix U95Av2 GeneChips (Affymetrix, Santa Clara, CA) featuring 12,625 transcripts. The procedures were conducted according to the supplier's protocols as described previously [10]. The arrays were scanned using the GeneArray scanner (Affymetrix) at 3-μm resolution, and the scanned image was analyzed quantitatively with the computer software Microarray Suite 4.0 (Affymetrix) to generate raw signal intensity data. In order to compare mRNA expression levels among samples, we normalized the raw data by setting the mean of the signal intensities of all probe sets to 1000 in each sample. The normalized signal intensity is referred to as AD (average difference) score. For statistical analysis to select genes, Microsoft Excel was used. First, microarray analyses were performed in 8 peritoneal wash samples from early gastric cancer patients and 12 gastric cancer cell lines. The eight peritoneal washings were used as negative control and the 12 cell lines as positive control to find genes specific to cancer cells. Seventy genes were extracted and then 46 gastric cancer tissues were also analyzed by microarray to exclude genes rarely expressed in primary gastric cancers. The finally selected genes were then validated by reverse transcription (RT)-PCR analyses in peritoneal washings from patients whose clinical outcome was followed up at least 2 years.

RT-PCR analysis in RNA samples from peritoneal washings. To overcome the limitation in the amount of samples needed for frequent RT-PCR analyses, we produced hundreds of micrograms of cDNA from 1 to 5 μg total RNA prepared from the peritoneal washings of 104 gastric cancer patients by an efficient method of high-fidelity mRNA amplification, called TALPAT [10]. RT-PCR was carried out in a total volume of 50 μl containing upstream and downstream primers (0.1 nmol each), 2.0 mM $MgCl_2$, 0.25 mM dNTP, 0.1 μg of the cDNA from each patient, and 2.5 U Ex *Taq* polymerase (Takara, Shiga, Japan).

The first PCR was cycled 25 times and another 15 cycles with 1/20 μl from the first PCR solution was added for nested PCR. For *CEA*, each cycle was heated at 95 °C for 1 min and 72 °C for 2.5 min, and for all of the other genes, 95 °C for 1 min, 55 °C for 1 min, and 72 °C for 1 min. PCR was cycled the above times followed by incubation at 72 °C for 10 min. The PCR products were separated by electrophoresis in 2%

Table 2
Frequency of expression in primary cancers

	All types ($n = 46$)	Intestinal type[a] ($n = 17$)	Diffuse type[b] ($n = 29$)	P value[c]
CK20	20 (43.5)	8 (47.1)	12 (41.4)	0.71
FABP1	25 (54.3)	11 (64.7)	14 (48.3)	0.28
MUC2	17 (37.0)	7 (41.2)	10 (34.5)	0.65
TFF1	45 (97.8)	16 (94.1)	29 (100)	0.19
TFF2	35 (76.1)	11 (64.7)	24 (82.8)	0.17
MASPIN	32 (69.6)	15 (88.2)	17 (58.6)	0.04
GW112	36 (78.3)	14 (82.4)	22 (75.9)	0.61
PRSS4	41 (89.1)	17 (100)	24 (82.8)	0.07
MDK	40 (87.0)	15 (88.2)	25 (86.2)	0.84
SOX9	43 (93.5)	17 (100)	26 (89.7)	0.17
CDX1	19 (41.3)	9 (52.9)	10 (34.5)	0.22

[a] Intestinal type includes well and moderately differentiated adenocarcinoma.

[b] Diffuse type includes poorly differentiated adenocarcinoma and signet ring cell carcinoma.

[c] The proportional differences were calculated by χ^2 test.

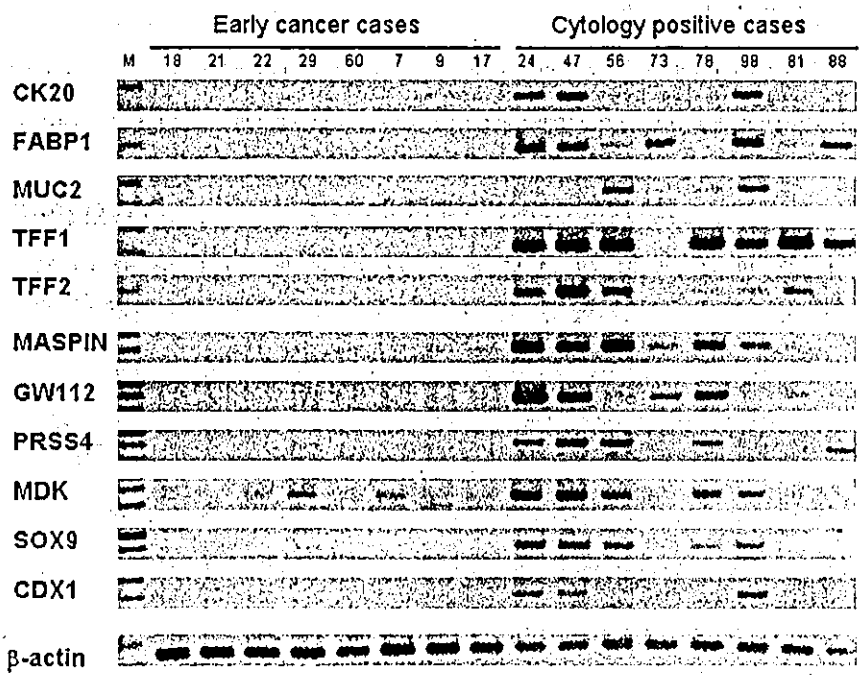

Fig. 1. Results of RT-PCR on peritoneal washings. The mRNAs of five genes, *CK20*, *FABP1*, *MUC2*, *TFF1*, and *TFF2*, were detected in most of the cytology-positive cases, but in none (except for TFF1) of the eight early gastric cancer cases even after a nested PCR. The other genes, *MASPIN*, *GW112*, *PRSS4*, *MDK*, *SOX9*, and *CDX1*, also showed correct results by a single PCR. The integrity of extracted RNA was confirmed by RT-PCR of *β-actin* mRNA. Top of each lane: M, a size marker, and each number, a sample No.

agarose gel, stained with ethidium bromide, and visualized under ultraviolet transilluminator. Primer sequences are shown in Table 1.

Statistical analyses. Survival analyses were made by Kaplan–Meier curves with the diagnosis of disease recurrence as the endpoints.

Results

The peritoneal washings from gastric cancer patients contain erythrocytes, leukocytes, dissociated peritoneal mesothelium, and a small number of cancer cells. Therefore, genes, which express in cancer cells but not in leukocytes or the mesothelium, are considered to be targets for detecting minimal gastric cancer cells in peritoneal washings. The first step of gene selection using a microarray of 12,625 transcripts left 70 genes whose mRNAs were not only undetectable (AD score corresponding to a signal intensity is below 500) in the peritoneal washes of all the eight early gastric cancer patients, but also abundant (AD score higher than 5000) in at least one of the 12 gastric cell lines. *CEA* did not fulfill this requirement because the AD score exceeded the threshold of 500 in only one peritoneal wash sample. In the second step, 40 genes out of the 70 were selected considering their known functions, tissue specificity, and expression levels in the primary gastric cancer tissues. The final step for the 40 genes, in which 16 representative peritoneal wash samples derived from both eight early cases and eight cytology-positive cases were analyzed by RT-PCR, yielded 11 genes whose mRNAs were detected in the cytology-positive cases but not in the early gastric cancers. Among them, mRNAs of five genes, *TFF1* (except for No. 17), *TFF2*, *FABP1*, *CK20*,

Table 3
Cytology and RT-PCR results in 99 patients

Cytology	Incurable disease (*n*)	CK20	FABP1	MUC2	TFF1	TFF2	Two or more of five genes	CEA
Positive (18)	Peritoneal	10	12	7	15	13	15	17
Negative[a]	None[b] (55)	0	3	0	5	4	1	10
	Peritoneal (9)	4	4	3	3	2	4	7
	Non-peritoneal metastasis (13) (recurrence)	2	5	1	7	4	4	7
	Proportional differences[c]	<0.04	0.005	0.19	0.0009	<0.04	0.004	0.013
	Non-peritoneal metastasis (3) (synchronous)	0	0	0	0	1	0	1
	Unresectable (1)	1	0	0	0	0	0	1
Overall specificity to incurable cases (%)		100	95	100	91	93	98[b]	82
Sensitivity to cytology positive cases (%)		56	67	39	83	72	83	94

[a] Including clinically early stage cases for which cytology was not performed.
[b] Two cases for TFF1 and CEA and one for TFF2 developed recurrence after 2 years. The only case positive for more than two markers also had peritoneal recurrence and, accordingly, the specificity to incurable cases was 100% finally.
[c] Proportional differences between non-peritoneal recurrence and recurrence free group. One-sided Fisher's exact test.

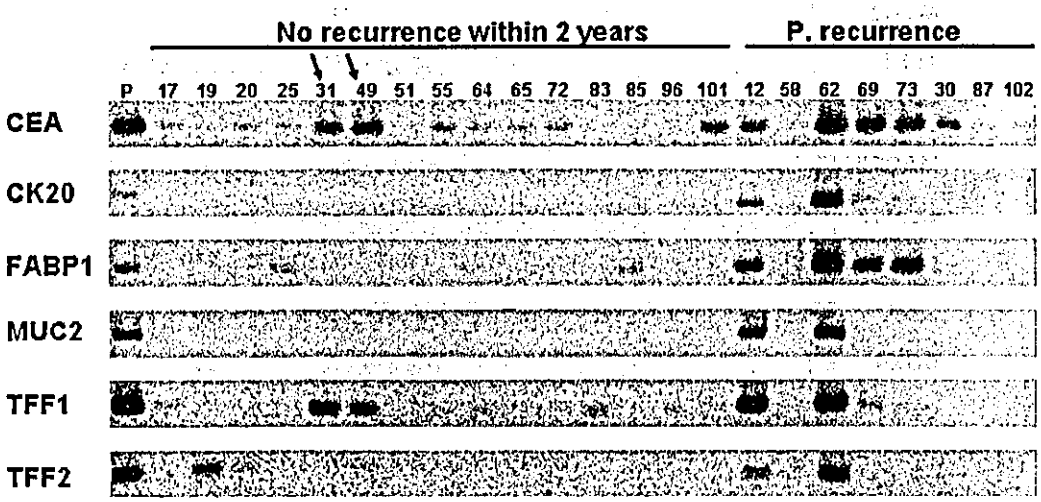

Fig. 2. Representative RT-PCR results of the five type A genes and *CEA* in peritoneal washings of 99 gastric cancer patients. Ten positive cases for *CEA* (18%) were observed in the 55 patients who had no incurable factor and did not develop recurrence within 2 years, while there were no positive cases for *CK20* and *MUC2* (0%), 3 for *FABP1* (5%), 4 for *TFF2* (7%), and 5 for *TFF1* (9%). Two cases (No. 31 and 49) eventually had recurrence after more than 900 days (arrow).

and *MUC2* were not detectable in the eight early cases even after a nested PCR (Fig. 1). The other genes, *MASPIN*, *GW112*, *PRSS4*, *MDK*, *SOX9*, and *CDX1*, also showed correct results by a single PCR but produced positive bands in the early cases by nested PCR. The frequency of their expression in the 46 gastric cancer tissues by microarray analyses is shown in Table 2. Almost none of these 11 genes had a significant difference in their frequency between intestinal-type and diffuse-type cancers, suggesting that these genes can be markers detecting gastric cancer cells derived from either major type of gastric cancer.

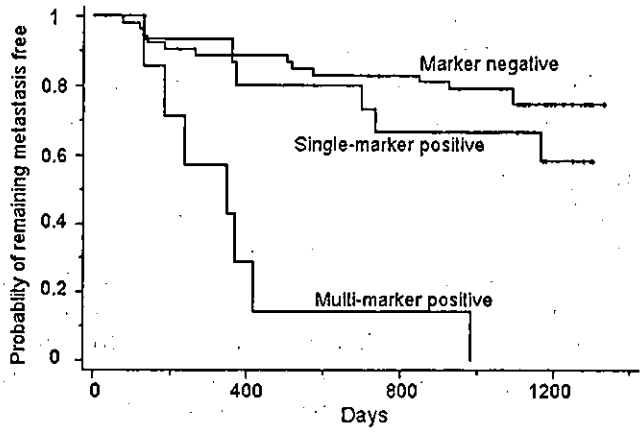

Fig. 3. Disease outcome of 75 potentially curative patients without synchronous metastases or positive cytology. Probability of metastases was significantly different among groups classified according to the result of RT-PCR with the five markers identified in this study (log-rank test, $P < 0.0001$).

Next, expression of the former five genes together with *CEA* was examined by nested PCR in the 99 peritoneal wash samples. Table 3 shows the number of positive results in each group of patients divided according to their cytology and disease outcome. Fifty-five patients were free from disease recurrence within 2 years after surgery and positive results in this group were 10 for *CEA* and 0–5 for the five genes identified in this study. Thus the specificity of the 5 genes identified in this study to early recurrence was 91–100%. Multiple (two or more) positive results with the five genes (not including *CEA*) were far more reliable and produced better specificity and sensitivity and, therefore, may be defined as high-risk of recurrence. The specificity may be improved with further followup and, actually, two additional cases

Table 4
Clinical outcome and disease stage of 24 patients with two or more positive RT-PCR results

Cases	Tumor depth	Nodal metastases[a]	Main metastatic site	DFS[b]	CK20	FABP1	MUC2	TFF1	TFF2
1	T2	10/45	Peritoneum	986	–	–	–	+	+
2	T3	16/84	Peritoneum	239	+	+	–	+	–
3	T3	19/75	Peritoneum	348	+	+	+	+	+
4	T2	9/73	Liver	183	–	+	–	+	–
5	T2	41/64	Liver	369	–	+	–	+	+
6	T3	9/78	Lung	418	+	+	–	+	+
7	T3	27/70	Systemic[c]	130	+	+	+	+	+
				CY,[d] P					
8	T3	28/37	Lymph nodes[e]	CY+, P–	–	–	–	+	+
9	T3	46/59	Peritoneum	CY+, P–	–	+	–	+	+
10	T3	27/59	Peritoneum	CY+, P–	–	+	–	+	+
11	T3	5/84	Peritoneum	CY+, P–	+	+	–	+	–
12	T4	22/33	Peritoneum	CY+, P–	+	+	–	+	+
13	T3	50/84	Systemic[c]	CY+, P–	+	–	+	+	+
14	T3	9/48	Peritoneum	CY+, P+	+	+	–	–	–
15	T3	16/47	Peritoneum	CY+, P+	–	+	–	+	+
16	T4	23/51	Peritoneum	CY+, P+	–	–	+	+	+
17	T3	0/4	Peritoneum	CY+, P+	+	+	–	+	+
18	T4	—	Peritoneum	CY+, P+	+	+	+	+	+
19	T4	—	Peritoneum	CY+, P+	+	+	+	+	+
20	T3	11/44	Peritoneum	CY+, P+	+	+	+	+	+
21	T3	—	Peritoneum	CY+, P+	+	+	+	+	+
22	T3	18/21	Peritoneum	CY+, P+	+	+	+	+	+
23	T4	25/62	Peritoneum	CY–, P+	+	+	+	–	–
24	T3	18/40	Peritoneum	CY–, P+	+	+	+	+	+

[a] Metastatic/investigated nodes.
[b] Disease free survival (days).
[c] Multifocal hematogenous metastasis was observed but no evident peritoneial disease.
[d] Cytology and macroscopic peritoneal nodules.
[e] Obstructive jaundice due to metastatic nodes in hepatoduodenal membrane.

of recurrence were observed in the RT-PCR positive cases after more than 900 days after surgery (Table 3 and Fig. 2). The impact of these markers on the disease outcome after potentially curative surgery was shown by the Kaplan–Meier curves and log-rank test (Fig. 3). Patients with multiple-positive results with these five genes had a significantly poorer prognosis than the rest of the patients.

Interestingly, a notably high proportion of positive results was observed in the non-peritoneal recurrence group (Table 3, one sided Fisher's exact test, $p = 0.19$–0.0009). Table 4 shows all cases with multiple positive results and the pathological stage and disease outcome of such cases. Most cases had evident or retrospectively proven peritoneal free cancer cells but four hematogenous recurrences were observed among them. It may be safely presumed that these four patients initially had minimal residual disease in their peritoneal cavity that could have predicted disease recurrence. RT-PCR with the combination of five genes was able to detect 6 out of 20 additional cases of early recurrence that the conventional method was unable to predict. Moreover, out of 29 incurable cases without synchronous macroscopic incurable factor (such as peritoneal nodules and/or liver metastasis), this method alone could predict 12 cases whereas conventional cytology alone identified nine cases.

Fig. 2 shows all RT-PCR positive results for patients without early recurrence and with peritoneal recurrence after negative cytology. Cases 31 and 49 eventually developed peritoneal recurrence (disease free survival = 986 days) and Krukenberg Tumor (disease free survival = 1167), respectively, after a long occult disease stage period. The rest of the positive bands in the no-recurrence group were generally very weak.

Discussion

Microarray technique has been reported to have a great potential for identifying genes able to classify phenotypically identical tumors [11,12] or predict tumor sensitivity to chemotherapeutic or hormonal agents [13,14]. Our present study demonstrated that this technique is also a very useful tool for identifying molecular markers for detecting minimal residual disease.

Other analyses directly comparing the gene expression of peritoneal washings from eight early gastric cancer and four cytology positive cases yielded a set of inflammation-associated genes; however, RT-PCR analyses on these genes including *GRO3*, *SCYA20*, and *PTSG2* failed on identification of marker genes specific to cytology positive samples.

FABP1/L-FABP encodes the liver fatty acid binding protein and is expressed only in the epithelial absorptive cells of the duodenum, jejunum, ileum, and colon, but not in the esophagus and stomach, while its mRNA expression in gastric cancer has not been reported yet [15]. Accordingly, our data are the first to show the frequent expression of *FABP1* in gastric cancers. CK 7 and CK 20 are reportedly potentially useful markers for an immunohistochemical study to rule out patients with a high risk of Barrett's esophagus and cancer [16], and CK20 for the detection of lymph node micrometastases in patients with gastric cancer [5]. A subset of gastric cancers has been reported to express *TFF1*, *TFF2*, and *MUC2* mRNAs [17].

It is quite interesting that 13 patients with non-peritoneal recurrences in the potentially curative patients frequently showed positive results by RT-PCR. It is a generally accepted concept that the tumor cells dissociated from the primary lesions do not always form metastatic lesions [18]. To form a peritoneal metastasis, tumor cells need to survive after the dissociation from the primary lesion. In gastric cancer, the expression of integrin $\alpha 6\beta 4$ was shown to induce apoptosis of gastric cancer cell lines injected into mouse peritoneal cavity and that its expression in gastric cancer inversely correlated with the frequency of peritoneal metastases [19]. In the cases that developed non-peritoneal recurrence, we may have detected gastric cancer cells that could not survive in the peritoneal cavity long enough to form peritoneal metastases. The detection of free cancer cells in the peritoneal cavity does not necessarily predict peritoneal recurrence but may well be interpreted as their malignant potential characterized by the resistance to apoptosis induced by the dissociation from the primary lesion.

The present results demonstrate that nested RT-PCR on the peritoneal washings using multiple genes is a specific and sensitive tool for detecting rare gastric cancer cells in the peritoneal cavity, so that gastric cancer patients are able to receive more suitable individualized therapies. Benefits from adjuvant therapies or radical surgery are still a matter of controversy [20–23]. However, most past clinical trials were designed for non-stratified patients and thus may have buried the potential benefit of adjuvant therapies confined to the very early stage of metastatic disease. Patients with minimal residual disease after sufficient local control may be the most eligible patients for clinical trials of post-operative adjuvant chemotherapy. After confirmation of our findings, future clinical trials featuring the molecular markers identified in this study may be of great importance in finding out more suitable treatment strategies for gastric cancer patients.

Acknowledgments

We thank Mr. K. Nomoto (Clinical Laboratory Division, National Cancer Center Hospital) for his excellent technical assistance in

conventional cytology. This work was supported by a Grant-in-Aid for the Second Comprehensive 10-Year Strategy for Cancer Control from the Ministry of Health, Labor and Welfare of Japan; and by the Program for the Promotion of Fundamental Studies in Health Science of the Organization for Pharmaceutical Safety and Research of Japan. K. Mori is an awardee of Research Resident Fellowships from the Foundation for Promotion of Cancer Research.

References

[1] E. Evron, W.C. Dooley, C.B. Umbricht, et al., Detection of breast cancer cells in ductal lavage fluid by methylation-specific PCR, Lancet 357 (2001) 1335–1336.
[2] G. Traverso, A. Shuber, B. Levin, et al., Detection of APC mutations in fecal DNA from patients with colorectal tumors, N. Engl. J. Med. 346 (2002) 311–320.
[3] Y. Kodera, H. Nakanishi, S. Ito, et al., Quantitative detection of disseminated free cancer cells in peritoneal washes with real-time reverse transcriptase-polymerase chain reaction, Ann. Surg. 235 (2002) 499–506.
[4] T. Fujimura, T. Ohta, H. Kitagawa, et al., Trypsinogen expression and early detection for peritoneal dissemination in gastric cancer, J. Surg. Oncol. 69 (1998) 71–75.
[5] Y. Okada, Y. Fujiwara, H. Yamamoto, et al., Genetic detection of lymph node micrometastases in patients with gastric carcinoma by multiple-marker reverse transcriptase-polymerase chain reaction assay, Cancer 92 (2001) 2056–2064.
[6] H. Katai, K. Maruyama, M. Sasako, et al., Mode of recurrence after gastric cancer surgery, Dig. Surg. 11 (1994) 99–103.
[7] M. Gerhard, H. Juhl, H. Kalthoff, et al., Specific detection of carcinoembryonic antigen-expressing tumor cells in bone marrow aspirates by polymerase chain reaction, J. Clin. Oncol. 12 (1994) 725–729.
[8] M.G. Piva, F. Navaglia, D. Basso, et al., CEA mRNA identification in peripheral blood is feasible for colorectal, but not for gastric or pancreatic cancer staging, Oncology 59 (2000) 323–328.
[9] K. Nagao, H. Hisatomi, H. Hirata, et al., Expression of molecular marker genes in various types of normal tissue: implication for detection of micrometastases, Int. J. Mol. Med. 10 (2002) 307–310.
[10] K. Aoyagi, T. Tatsuta, M. Nishigaki, et al., A faithful method for PCR-mediated global mRNA amplification and its integration into microarray analysis on laser-captured cells, Biochem. Biophys. Res. Commun. 300 (2003) 915–920.
[11] J. Khan, J.S. Wei, M. Ringner, et al., Classification and diagnostic prediction of cancers using gene expression profiling and artificial neural networks, Nat. Med. 7 (2001) 673–679.
[12] F.M. Selaru, Y. Xu, J. Yin, et al., Artificial neural networks distinguish among subtypes of neoplastic colorectal lesions, Gastroenterology 122 (3) (2002) 606–613.
[13] C. Kihara, T. Tsunoda, T. Tanaka, et al., Prediction of sensitivity of esophageal tumors to adjuvant chemotherapy by cDNA microarray analysis of gene-expression profiles, Cancer Res. 61 (2001) 6474–6479.
[14] L.J. van 't Veer, H. Dai, M.J. van de Vijver, et al., Gene expression profiling predicts clinical outcome of breast cancer, Nature 415 (2002) 530–536.
[15] Y. Sakai, Quantitative measurement of liver fatty acid binding protein in human gastrointestinal tract, Nippon Shokakibyo Gakkai Zasshi 87 (1990) 2594–2604.
[16] A. Couvelard, J.M. Cauvin, D. Goldfain, et al., Cytokeratin immunoreactivity of intestinal metaplasia at normal oesophagogastric junction indicates its aetiology, Gut 49 (2001) 761–766.
[17] J.C. Machado, A.M. Nogueira, F. Carneiro, et al., Gastric carcinoma exhibits distinct types of cell differentiation: an immunohistochemical study of trefoil peptides (TFF1 and TFF2) and mucins (MUC1, MUC2, MUC5AC, and MUC6), J. Pathol. 190 (2000) 437–443.
[18] C. Marth, J. Kisic, J. Kaern, et al., Circulating tumor cells in the peripheral blood and bone marrow of patients with ovarian carcinoma do not predict prognosis, Cancer 94 (2002) 707–712.
[19] Y. Ishii, A. Ochiai, T. Yamada, et al., Integrin $\alpha 6\beta 4$ as a suppressor and a predictive marker for peritoneal dissemination in human gastric cancer, Gastroenterology 118 (2000) 497–506.
[20] D.H. Roukos, Current status and future perspectives in gastric cancer management, Cancer Treat. Rev. 26 (2000) 243–255.
[21] K. Shimada, J.A. Ajani, Adjuvant therapy for gastric carcinoma patients in the past 15 years: a review of western and oriental trials, Cancer 86 (1999) 1657–1668.
[22] J.J. Bonenkamp, J. Hermans, M. Sasako, et al., Extended lymph-node dissection for gastric cancer. Dutch Gastric Cancer Group, N. Engl. J. Med. 340 (1999) 908–914.
[23] J.S. Macdonald, S.R. Smalley, J. Benedetti, et al., Chemoradiotherapy after surgery compared with surgery alone for adenocarcinoma of the stomach or gastroesophageal junction, N. Engl. J. Med. 345 (2001) 725–730.

CT Findings of Surgically Resected Large Cell Neuroendocrine Carcinoma of the Lung in 38 Patients

Yasuji Oshiro[1]
Masahiko Kusumoto[2]
Yoshihiro Matsuno[3]
Hisao Asamura[4]
Ryousuke Tsuchiya[4]
Hiroshi Terasaki[5]
Hidefumi Takei[3]
Arafumi Maeshima[6]
Sadayuki Murayama[1]
Noriyuki Moriyama[2]

OBJECTIVE. We sought to assess the CT features of surgically resected large cell neuroendocrine carcinoma of the lung.

MATERIALS AND METHODS. The cases of all patients who underwent surgical resection for primary lung cancer in a single institution from 1993 to 2000 and who received an initial diagnosis of poorly differentiated non–small cell lung carcinoma, small cell carcinoma, carcinoid tumor, and large cell neuroendocrine carcinoma were histologically reviewed. The findings for 43 patients were histologically reclassified and confirmed as large cell neuroendocrine carcinoma. The CT scans available for 38 patients were evaluated by two observers.

RESULTS. In the 38 patients, six central tumors and 32 peripheral tumors, with diameters ranging from 12 to 92 mm (mean ± SD, 32 ± 19 mm), were identified. None of the tumors had air bronchograms or calcification in the mass or nodule. Of the 19 patients with thin-section CT scans, 14 (74%) showed the tumor–lung interface as well defined and five (26%) showed the interface to be ill defined. Lobulation was identified on 15 scans (79%) and spiculation was evident on six scans (32%). On contrast-enhanced CT scans, inhomogeneously enhanced tumors appeared to be larger (51 ± 18 mm) than homogeneously enhanced tumors (25 ± 10 mm; $p < 0.001$). At histopathologic examination, gross necrosis was noted in 20 of 28 patients who had undergone contrast-enhanced CT, and the cause of inhomogeneous enhancement on CT scans was determined to be intratumoral necrosis. Multiple microscopic necroses were present in all 28 patients.

CONCLUSION. Large cell neuroendocrine carcinoma usually appears as a well-defined and lobulated tumor with no air bronchograms or calcification. The inhomogeneous enhancement (caused by necrosis) seen in large cell neuroendocrine carcinomas with large diameters is not necessarily apparent in small-diameter (< 33 mm) large cell neuroendocrine carcinomas, even if the tumor contains necrosis.

Received December 20, 2002; accepted after revision July 10, 2003.

[1]Department of Radiology, University of Ryukyus School of Medicine, 207 Uehara, Nishihara-cho, Okinawa Prefecture 903-0215, Japan.

[2]Diagnostic Radiology Division, National Cancer Center Hospital, 1-1 Tsukiji 5-chome, Chuou-ku, Tokyo 104-0045, Japan. Address correspondence to M. Kusumoto.

[3]Clinical Laboratory Division, National Cancer Center Hospital, Tokyo 104-0045, Japan.

[4]Thoracic Surgery Division, National Cancer Center Hospital, Tokyo 104-0045, Japan.

[5]Department of Radiology, Kurume University School of Medicine, 67-Asahimachi, Kurume 830-0011, Japan.

[6]Pathology Division, National Cancer Center Research Institute, 1-1 Tsukiji 5-chome, Chuou-ku, Tokyo 104-0045, Japan.

AJR 2004;182:87–91

0361–803X/04/1821–87

In the revised World Health Organization (WHO) classification of lung cancer published in 1999, large cell neuroendocrine carcinoma was categorized as a variant of large cell carcinoma [1]. Large cell neuroendocrine carcinoma of the lung is defined as a poorly differentiated and high-grade neuroendocrine tumor that morphologically and biologically may be placed between atypical carcinoid tumor and small cell carcinoma [2]. Some researchers have reported that survival rates for patients with large cell neuroendocrine carcinoma are lower than those for patients with comparable stage I non–small cell lung carcinoma [3] or classic large cell carcinoma [4] and are no different than those for patients with small cell carcinoma [5]. Large cell neuroendocrine carcinomas of the lung have been more frequently studied in recent years; however, the number of patients with large cell neuroendocrine carcinoma is still relatively small in comparison to the numbers of patients with squamous cell carcinoma, adenocarcinoma, or small cell carcinoma. Several reports have described the pathologic and clinical features of large cell neuroendocrine carcinomas, but information on the imaging characteristics of these carcinomas is limited [6, 7]. For this reason, we analyzed the CT findings of 38 patients with resected large cell neuroendocrine carcinomas to determine the CT characteristics of these tumors and to identify any specific imaging features that may help in the diagnosis of the disease.

Materials and Methods

Between 1982 and 1999, 2,790 patients underwent surgical resection for primary lung carcinoma at the National Cancer Center Hospital. To

extract cases of large cell neuroendocrine carcinoma from this large pool of patients, we reviewed the records of 572 patients who had received one of the following histologic diagnoses: small cell carcinoma, poorly differentiated adenocarcinoma, poorly differentiated squamous cell carcinoma, large cell carcinoma, carcinoid tumor, and large cell neuroendocrine carcinoma. Three pathologists independently reviewed each case, resolving discrepancies among their findings by consensus. Immunohistochemical tests were performed on retained specimens to confirm the neuroendocrine phenotype in every patient. The details of histopathologic review of the cases have been described previously [3].

In 87 of the 572 patients, the carcinomas were reclassified and confirmed as large cell neuroendocrine carcinomas. CT scans were available for review in 34 of the 38 patients who underwent surgery during the most recent 7 years of the study period (1993–1999). In addition, we identified four patients with a histologically determined diagnosis of large cell neuroendocrine carcinoma who had undergone CT in 2000. Therefore, our study population consisted of 38 patients, 36 men and two women, whose ages ranged from 45 to 82 years (mean, 66 years). Of the 38 patients, 20 had lesions classified as large cell neuroendocrine carcinomas at the initial diagnosis. The initial pathologic diagnoses of the lesions in the remaining 18 patients were as follows: eight small cell carcinomas (six intermediate cell type), seven poorly differentiated adenocarcinomas, two large cell carcinomas, and one poorly differentiated squamous cell carcinoma. Thirty-one of 38 patients who presented without pulmonary symptoms had abnormal findings on chest radiographs obtained during a routine examination. Symptoms in the remaining seven patients included low-grade fever ($n = 1$), chest and back pain ($n = 1$), hemosputum ($n = 3$), and cough ($n = 2$). Thirty-one patients had been smokers for between 12 and 200 pack-years (mean, 62 pack-years). Six patients had quit smoking 3–17 years (mean, 7 years) before diagnosis. In one patient, a smoking history could not be obtained. Surgical procedures included a partial resection of the mass in four patients, segmentectomy in one patient, lobectomy in 27 patients, and pneumonectomy with regional lymph node dissection in six patients.

TABLE 1 CT Findings in 38 Patients with Surgically Resected Large-Cell Neuroendocrine Carcinomas

Finding	Patients	
	No.	%
Tumor location in lobe		
Peripheral	32	84
Central	6	16
Tumor location by lobe		
Right		
Upper	12	32
Middle	3	8
Lower	8	21
Left		
Upper	12	32
Middle	0	0
Lower	3	8
Internal characteristics		
Air bronchogram	0	0
Calcification	0	0
Cavity	1	3
Other findings		
Endobronchial growth	2	5
Obstructive pneumonia	3	8
Pleural effusion	9	24
Tumor–lung interface features[a]		
Well-defined	14	74
Ill-defined	5	26
Smooth	1	5
Lobulated	15	79
Spiculated	6	32
Ground-glass opacity	3	16
Surrounding emphysema[a]	4	21

Note.—Average tumor size ± SD = 32 ± 19 mm.

[a]These findings apply only to the 19 patients who underwent thin-section CT.

CT scans were obtained with X-Vigor or TCT-900S units (Toshiba, Tokyo, Japan). The helical technique (collimation, 10 mm; pitch, 1.5) was used and covered the area from the lung apices to the diaphragm. In 28 patients, nonionic iodinated contrast material (Iopamiron [iopamidol 300 mg I/mL], Nihon Schering, Osaka, Japan) was administered IV at a rate of 1–2 mL/sec. Contrast-enhanced CT scans were obtained within 120 sec (range, 70–120 sec) after the onset of contrast material infusion. Unenhanced scans were obtained in 20 of 28 patients who underwent contrast-enhanced CT. In 19 of 38 patients, additional thin-section (collimation, 2.0 mm; pitch, 1.0) scans were obtained at the level of the lesion. All CT scans were obtained with 120 kVp and 200 mA. The scans were viewed on standard mediastinal window setting (window level, 60 H; window width, 550 H) and lung window setting (window level, −600 H; window width, 1500–2000 H). The CT scans were assessed by two radiologists who reached conclusions by consensus.

CT scans were reviewed for location, size, and internal characteristics of the tumor. The descriptions of tumor location included identification of the affected lung lobe and of the position—central versus peripheral—of the tumor in the lobe. Central tumors were defined as those that involved the carina or a main segmental bronchus. Peripheral tumors were defined as those surrounded by lung parenchyma or distal to the subsegmental bronchi. The scans were evaluated for the presence of endobronchial growth, obstructive pneumonia or atelectasis, and pleural effusion. On thin-section CT, tumor–lung interface characteristics were assessed and the presence or absence of surrounding emphysema was noted.

Enhancement of the nodules was assessed subjectively by comparing the enhancement of the chest wall muscle on the unenhanced scans with corresponding enhancement on the contrast-enhanced scans. The enhancement patterns of the nodules were noted as either homogeneous or inhomogeneous. Inhomogeneity was defined as the presence of an area of low attenuation in the highly attenuated background of the nodule. Nodules with peripheral rim enhancement were also considered to have inhomogeneous enhancement. For the 28 patients who underwent contrast-enhanced CT, we reviewed the pathologic reports to identify those patients whose reports mentioned that necrosis was present in gross specimens and then correlated the presence of necrosis with the CT findings. Statistical analyses of size and macroscopic necrosis between homogeneously and inhomogeneously enhanced tumors were performed using Student's t test and Fisher's exact test, respectively. Mediastinal or hilar lymph nodes that were larger than 1 cm in the short-axis diameter were regarded as evidence of lymphadenopathy. Tumors were staged according to the TNM classification scheme [8]. No patients had extrathoracic metastases at the time of diagnosis. Distribution of the clinical stages was as follows: stage IA ($n = 20$); stage IB ($n = 7$); stage IIA ($n = 1$); stage IIB ($n = 3$); stage IIIA ($n = 5$); and stage IIIB ($n = 2$). The CT findings regarding the tumor–lung interface and intratumoral necrosis were correlated with findings at surgery and pathologic examination.

Results

The CT findings of large cell neuroendocrine carcinomas are summarized in Table 1. The right lung was involved in 23 (61%) and the upper lobes were involved in 24 (63%) of the 38 patients studied. The tumors were seen peripherally in 32 patients (84%) and centrally in six patients (16%). Endobronchial growth and obstructive pneumonia were associated only in patients with centrally located tumors. Neither air bronchograms nor calcification was observed in any patient.

Among the 19 patients who underwent thin-section CT, the more common tumor–lung interface characteristics were a well-defined interface (74%) and lobulation (79%) (Fig. 1). Spiculation (Figs. 2 and 3) was observed in six patients (32%). In four patients, however, spiculated margins appeared as fibrotic strands because of paracicatricial emphysema or linear opacities made more pronounced by preexisting emphysema (Fig. 2).

On contrast-enhanced CT, attenuation of all the tumors varied from slightly less than to more than the attenuation of the chest wall muscle. Among the 28 patients who had contrast-enhanced CT, 15 (54%) had tumors with

homogeneous enhancement (Figs. 2 and 3), and 13 tumors (46%) showed inhomogeneous enhancement. Of the inhomogeneously enhanced tumors, five had peripheral rim enhancement. As shown in Table 2, the inhomogeneously enhanced tumors were generally larger than the homogeneously enhanced tumors. At gross pathology examination of the resected tumors, necrosis was identified in seven of the 15 homogeneously enhanced carcinomas and in all of the 13 inhomogeneously enhanced carcinomas (Table 2). The largest homogeneously enhanced tumor with necrosis was 33 mm.

At histopathologic examination, pulmonary alveoli were filled entirely with tumor cells or had a compressive growth pattern, giving the appearance of a well-defined margin. Lobulated margins observed on CT reflected the interruption of tumor growth by anatomic structures or tumor extension due to differential tumor growth. In four patients, spiculation was attributable to paracicatricial or preexisting emphysema. In all other patients, spiculation corresponded to vascular and lymphatic invasion, a normal vascular structure, a thickened interstitium, or an irregularly protuberant tumor nest. In two patients, tumors associated with the bronchial wall were identified as endobronchial polypoid lesions that invaded the surrounding lung parenchyma. In one of the two patients, the invading lesion was accompanied by obstructive pneumonia. The cause of inhomogeneous enhancement was intratumoral necrosis.

Necrosis was noted in the gross pathology specimens of 20 of 28 patients who had contrast-enhanced CT scans. The difference between homogeneously and inhomogeneously enhanced tumors in the incidence of macroscopic necrosis was statistically significant ($p < 0.003$). Although the gross necrotic area was difficult to determine in the cut surface of the small tumors, multiple punctate necroses were observed microscopically in each case. In the large tumors, necrotic foci were larger and tended to be confluent. Consequently, the tumors contained extensive necroses. Inhomogeneous enhancement with peripheral rim enhancement represented a large central necrosis.

Discussion

The classification of pulmonary neuroendocrine tumors of the lung is complex and potentially confusing. For many years, carcinoid tumors and small cell lung carcinomas were the only two recognized types of these tumors. In 1972, Arrigoni et al. [9] proposed that bronchial carcinoid tumors be separated into typical and atypical variants, with the latter having more malignant histologic characteristics and clinical manifestations. Since then, neuroendocrine tumors of the lung have been frequently classified into three categories: typical carcinoid, atypical carcinoid, and small cell carcinoma [2, 10]. Most tumors classified morphologically as being between typical carcinoid tumor and small cell carcinoma have been called atypical carcinoids. However, these tumors were too heterogeneous to be grouped into a single category. Subsequently, Travis et al. [10] proposed a fourth category, large cell neuroendocrine carcinoma, which is characterized by a poorly differentiated and high-grade neuroendocrine tumor of the non–small cell type. Large cell neuroendocrine carcinomas have been categorized as being between atypical carcinoids and small cell carcinomas in terms of clinical aggressiveness [2, 5, 11].

The incidence of large cell neuroendocrine carcinoma in cases of resectable primary lung cancers is 2.8–3.1% [2, 3]. The clinical features of the 38 patients with large cell neuroendocrine carcinoma in our study—the mean age, predominance of men, and strong association with smoking—were similar to those previously documented in the literature [2, 10]. However, 31 patients (82%) were asymptomatic and had large cell neuroendocrine carcinoma detected incidentally, which is a larger percentage than the percentages previously reported [6, 7]. This difference is presumably due to the number of patients with earlier stages of large cell neuroendocrine carcinoma in our study population.

Large cell neuroendocrine carcinomas have been reported as occurring in either central or peripheral locations [10]. Our experience supports a predominately peripheral location. In our series, large cell neuroendocrine carcinomas were slightly more common

Fig. 1.—Thin-section (2-mm collimation) CT scan obtained with lung window setting in right lower lobe of 77-year-old man with large cell neuroendocrine carcinoma shows well-defined lobulated nodule.

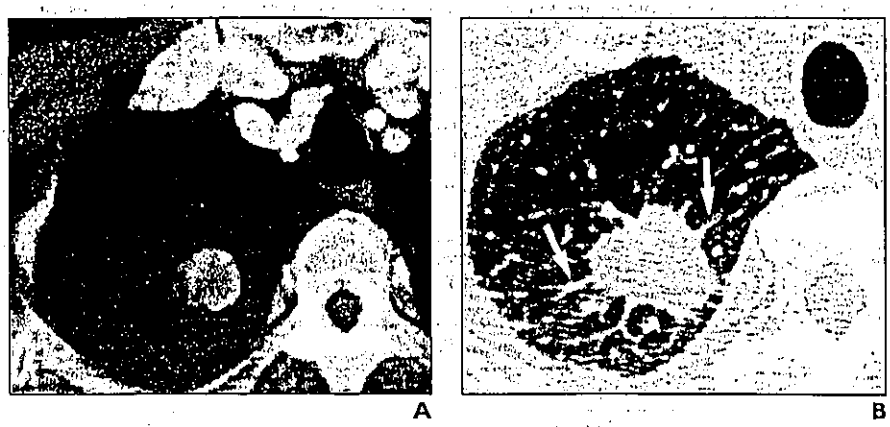

A B

Fig. 2.—Large cell neuroendocrine carcinoma in 71-year-old man.
A, Contrast-enhanced conventional 10-mm-thick CT scan obtained in right upper lobe shows round nodule with mild homogeneous enhancement.
B, Thin-section (2-mm collimation) CT scan obtained with lung window setting shows ill-defined spiculated nodule. Coarse spiculation (*arrows*) is evident around periphery of tumor with extension to pleural surface and into emphysematous lung.

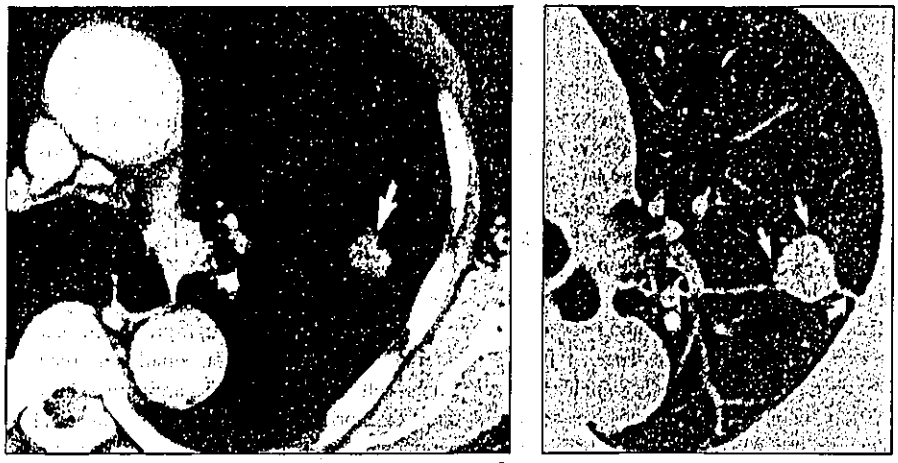

Fig. 3.—Large cell neuroendocrine carcinoma in 82-year-old man.
A, Contrast-enhanced conventional 10-mm-thick CT scan obtained in left upper lobe shows lobulated nodule (*arrow*) with mild homogeneous enhancement.
B, Thin-section (2-mm-collimation) CT scan obtained with lung window setting shows ill-defined spiculated nodule (*straight arrows*) with pleural indentation (*curved arrow*).
C, Photomicrograph of histopathologic specimen exhibits spiculated margins due to vascular invasion (*arrow*) and irregularly protuberant tumor nest (*arrowhead*). (H and E, ×3)

in the right lung than in the left and slightly more common in the upper lobe than in the middle or lower lobes. The reason for the higher incidence in these regions is uncertain; however, pulmonary carcinomas are known to occur with a relative frequency of 3:2 in the right versus left lung and in the upper versus lower lobe [12]. A well-defined and lobulated appearance without air bronchograms or calcification was the most common finding in the large cell neuroendocrine carcinomas observed in our study. These results are compatible with the recently reported descriptions of large cell neuroendocrine carcinoma [6, 7].

Jung et al. [7] reported that spiculation was present in eight (73%) of 11 cases of large cell neuroendocrine carcinoma. In our study, spiculation was found in six (32%) of 19 patients who had thin-section CT scans available. Spiculations are frequently seen in adenocarcinomas and occasionally in squamous cell carcinomas, corresponding to a diffuse desmoplastic response to tumor growth [13]. In our series, spiculated margins were caused by paracicatricial emphysema with extension into surrounding emphysematous lung or by linear opacities made more prominent by preexisting emphysema in four (67%) of the six tumors with spiculation. Because emphysema is thought to be caused by smoking, the spiculation of large cell neuroendocrine carcinomas in our study may be associated with the high incidence of smokers in our patients.

The scans of 13 of the 28 patients who had undergone contrast-enhanced CT showed inhomogeneous enhancement caused by gross intratumoral necrosis. Statistically, inhomogeneously enhanced tumors were larger than homogeneously enhanced tumors. Microscopic focal necrosis was present in each case, and the extent of necrosis varied considerably. In adenocarcinomas and squamous cell carcinomas, central necrosis is frequent and may be more extensive in larger tumors [12]. Similarly, in large-diameter large cell neuroendocrine carcinomas, the necrotic area seemed to be confluent and more extensive. Although small-diameter tumors contained macroscopic necrosis, they tended to show homogeneous enhancement. Identifying these necroses on contrast-enhanced CT was difficult because the necrotic foci were too small to be detected. Endobronchial growth has been associated with typical carcinoid tumors [12], but we observed it only infrequently in the large cell neuroendocrine carcinomas in our study. We found the incidence of postobstructive pneumonia or atelectasis on CT to be 8%, lower than the 27% (3/11 patients) reported by Jung et al. [7]. This difference in findings may be the result of infrequent central or endobronchial growth.

Before its new classification, large cell neuroendocrine carcinoma had been categorized in several ways. In reviewing previous cases seen in our institution, we noticed that some patients with large cell neuroendocrine carcinoma had formerly been diagnosed as having small cell carcinoma, adenocarcinoma, squamous cell carcinoma, or large cell carcinoma [3].

Radiographically, small cell carcinoma in most cases exhibits extensive hilar and mediastinal lymphadenopathy, and sometimes a primary pulmonary tumor is not recognized [12]. However, 5–10% of patients with small cell carcinoma have solitary pulmonary nodules [14–16]. Among eight patients in our study initially classified as having small cell carcinoma, six had been diagnosed as having

TABLE 2 Comparison of Macroscopic Necrosis and Tumor Size by Enhancement Pattern on Contrast-Enhanced CT in 28 Patients with Large Cell Neuroendrocrine Carcinoma

Feature	Enhancement Pattern		*p*
	Homogeneous	Inhomogeneous	
Macroscopic necrosis	7 of 15 patients	13 of 13 patients	< 0.003
Tumor size (mm)			
Mean ± SD	25 ± 10	51 ± 18	< 0.001
Range	13–54	20–92	

Note.—Overall mean tumor size ± SD was 32 ± 19 mm.

an intermediate cell type of the disease. Yabuuchi et al. [16] reported that on CT, peripheral small cell carcinoma displays a well-defined, rounded, or lobulated homogeneous mass. The CT features on the scans of our patients initially diagnosed as small cell carcinoma were similar to the CT features of peripheral small cell carcinoma described earlier. Large cell neuroendocrine carcinoma and peripheral small cell carcinoma also have similar pathologic and CT features. Thus, histologic review of peripheral small cell carcinoma cases should be performed using new WHO criteria because it is possible that some of the patients with currently accepted diagnoses of peripheral small cell carcinoma should be reclassified as having large cell neuroendocrine carcinoma.

Our study has some limitations. The CT findings in our study population may not reflect the findings in all patients with large cell neuroendocrine carcinoma because our study was limited to patients whose tumors were surgically resected. This substantial selection bias might explain the presence of peripheral tumors in so many of our patients. However, a diagnosis of large cell neuroendocrine carcinoma is usually based on a histologic findings in a specimen obtained by surgical resection, as was the case in our study. More research is needed to clarify large cell neuroendocrine carcinoma findings in all patients, including patients with large cell neuroendocrine carcinoma who are not treated surgically. Other limitations of our study include a reliance on visual estimation of the CT scans with no comparison of the region of interest in the tumor with that in unenhanced scans and the variation in both the IV contrast injection rates (range, 1–2 mL/sec) and scanning times (range, 70–120 sec), each of which may have affected the homogeneity of the tumor.

In conclusion, we found that large cell neuroendocrine carcinoma usually appeared as a well-defined and lobulated tumor without air bronchograms or calcification. Infrequently, this appearance was accompanied by spiculation due to paracicatricial or preexisting emphysema. We found that the CT findings of large cell neuroendocrine carcinomas were similar to those of other expansively growing tumors, such as peripheral small cell carcinomas, poorly differentiated adenocarcinomas, and squamous cell carcinomas. Large-diameter large cell neuroendocrine carcinomas tended to show inhomogeneous enhancement because of necrosis, but this type of enhancement was not necessarily apparent in small-diameter (< 33 mm) large cell neuroendocrine carcinomas, even if the tumors were necrotic.

References

1. Travis WD, Colby TV, Corrin B, et al. *Histopathologic typing of lung and pleural tumors*, 3rd ed. Berlin, Germany: Springer-Verlag, 1999:5–98
2. Jiang SX, Kameya T, Shoji M, Dobashi Y, Shinada J, Yoshimura H. Large cell neuroendocrine carcinoma of the lung: a histologic and immunohistochemical study of 22 cases. *Am J Surg Pathol* 1998;22:526–537
3. Takei H, Asamura H, Maeshima A, et al. Large cell neuroendocrine carcinoma of the lung: a clinicopathologic study of eighty-seven cases. *J Thorac Cardiovasc Surg* 2002;124:285–292
4. Iyoda A, Hiroshima K, Toyozaki T, Haga Y, Fujisawa T, Ohwada H. Clinical characterization of pulmonary large cell neuroendocrine carcinoma and large cell carcinoma with neuroendocrine morphology. *Cancer* 2001;91:1992–2000
5. Travis WD, Rush W, Flieder DB, et al. Survival analysis of 200 pulmonary neuroendocrine tumors with clarification of criteria for atypical carcinoid and its separation from typical carcinoid. *Am J Surg Pathol* 1998;22:934–944
6. Shin AR, Shin BK, Choi JA, Oh YW, Kim HK, Kang EY. Large cell neuroendocrine carcinoma of the lung: radiologic and pathologic findings. *J Comput Assist Tomogr* 2000;24:567–573
7. Jung KJ, Lee KS, Han J, et al. Large cell neuroendocrine carcinoma of the lung: clinical, CT, and pathologic findings in 11 patients. *J Thorac Imaging* 2001;16:156–162
8. Sobin LH, Wittenkind CH. *TNM classification of malignant tumors*, 5th ed. New York, NY: John Wiley & Sons, 1997:91–100
9. Arrigoni MG, Woolner LB, Bernatz PE. Atypical carcinoid tumors of the lung. *J Thorac Cardiovasc Surg* 1972;64:413–421
10. Travis WD, Linnoila RI, Tsokos MG, et al. Neuroendocrine tumors of the lung with proposed criteria for large cell neuroendocrine carcinoma: an ultrastructural, immunohistochemical, and flow cytometric study of 35 cases. *Am J Surg Pathol* 1991;15:529–553
11. Dresler CM, Ritter JH, Patterson GA, Ross E, Bailey MS, Wick MR. Clinical–pathologic analysis of 40 patients with large cell neuroendocrine carcinoma of the lung. *Ann Thorac Surg* 1997;63:180–185
12. Fraser R, Müller N, Colman N, Paré P. *Diagnosis of disease of the chest*, 3rd ed. Philadelphia, PA: Saunders, 1999:1067–1250
13. Sone S, Sakai F, Takashima S, et al. Factors affecting the radiologic appearance of peripheral bronchogenic carcinomas. *J Thorac Imaging* 1997;12:159–172
14. Quoix E, Fraser R, Wolkove N, Finkelstein H, Kreisman H. Small cell lung cancer presenting as a solitary pulmonary nodule. *Cancer* 1990;66:577–582
15. Gephardt GN, Grady KJ, Ahmad M, Tubbs RR, Mehta AC, Shepard KV. Peripheral small cell undifferentiated carcinoma of the lung: clinicopathologic features of 17 cases. *Cancer* 1988;61:1002–1008
16. Yabuuchi H, Murayama S, Sakai S, et al. Resected peripheral small cell carcinoma of the lung: computed tomographic-histologic correlation. *J Thorac Imaging* 1999;14:105–108

Grade of Stromal Invasion in Small Adenocarcinoma of the Lung

Histopathological Minimal Invasion and Prognosis

Hiroyuki Sakurai, MD,† Arafumi Maeshima, MD,‡ Shun-ichi Watanabe, MD,* Kenji Suzuki, MD,* Ryosuke Tsuchiya, MD,* Akiko M. Maeshima, MD,‡ Yoshihiro Matsuno, MD,† and Hisao Asamura, MD**

Abstract: The pathologic features of invasion such as stromal disruption and pleural/vascular involvement have been shown to be of prognostic value in adenocarcinoma. However, the relationship between the degree of invasion, histologic subtype of adenocarcinoma, and prognosis remains unclear. We retrospectively studied 380 peripheral adenocarcinomas of ≤2.0 cm in diameter with regard to histology and clinical profiles. Their degree of invasive growth was classified into four grades as follows according to the structural deformity and its location in the adenocarcinoma lesion: Grade 0 had a pure bronchioloalveolar growth pattern and no evidence of stromal invasion. Grade 1 had stromal invasion in the area of bronchioloalveolar growth. Grade 2 had stromal invasion localized on the periphery of a fibrotic focus. Grade 3 had stromal invasion into the center of a fibrotic focus. The clinicopathological data were obtained from medical records. The distribution of the histologic grade of invasion was as follows: grade 0 in 85 tumors (22%), grade 1 in 37 (10%), grade 2 in 46 (12%), and grade 3 in 212 (56%). This histologic grade of invasion was closely related to other indicators of tumor spread. Vascular/lymphatic permeation was seen in none of grade 0, in 1 lesion each of grade 1 and grade 2, and 144 (68%) of grade 3. Lymph node metastasis was seen in 57 (27%) lesions of grade 3 but not in grades 0, 1, or 2. The 5-year disease-free survival rates were 100%, 100%, 100%, and 59.6% for tumors with grade 0, grade 1, grade 2, and grade 3 invasion, respectively. Tumors with grade 1 and grade 2 invasion, like tumors with grade 0 invasion (bronchioloalveolar carcinoma), showed an excellent prognosis. Therefore, tumors with grade 1 and grade 2 invasion could be considered "minimally invasive" or "early" adenocarcinomas.

From the *Division of Thoracic Surgery and †Clinical Laboratory, National Cancer Center Hospital, and the ‡Pathology Division, National Cancer Center Research Institute, Tokyo, Japan.

Supported in part by a Grants-in-Aid for Cancer Research (11–19 and 12–5) from the Ministry of Health, Welfare, and Labor, Japan.

Reprints: Hisao Asamura, MD, Division of Thoracic Surgery, National Cancer Center Hospital 1-1, Tsukiji 5-chome, Chuo-ku, Tokyo 104-0045, Japan (e-mail: hasamura@ncc.go.jp).

Key Words: adenocarcinoma, pathology, prognosis, early cancer, lung

(*Am J Surg Pathol* 2004;28:198–206)

Because of the advent of high-resolution computed tomography (CT) and the consequent availability of more detailed images and screening programs, small lung cancers are being found more often.[12] Most of these have an adenocarcinoma histology and arise in the periphery of the lung parenchyma.[1] It has also been repeatedly reported that lymph node metastasis is found in approximately 20% of peripheral adenocarcinomas, even if the tumor diameter is small, such as <2.0 cm.[2,11,13,15,17,22]

On the other hand, another histologic category of adenocarcinoma, bronchioloalveolar carcinoma (BAC), has also been discussed with regard to its histologic features and prognosis.[5,6,8,14,23] This subcategory is classified as a subtype of adenocarcinoma, which histologically shows a unique replacing growth pattern of tumor cells along the alveolar wall. According to radiologic studies by high-resolution CT, the replacing growth pattern of adenocarcinoma cells seen in BAC presents as a focal, hazy increase in attenuation called "ground-glass opacity."[3] Radiologic-pathologic studies have demonstrated that the ground-glass opacity appearance represents patent alveolar spaces and the preservation of bronchial and vascular margins.[16,18]

In the recently revised histologic classification of lung and pleural tumors by the World Health Organization (WHO),[29] adenocarcinomas have been classified into five histologic subtypes: BAC, acinar, papillary, solid with mucin, and adenocarcinoma with mixed subtypes. The WHO classification describes BAC as a form of adenocarcinoma with a pure bronchioloalveolar growth pattern and no evidence of stromal, vascular, or pleural invasion. Accordingly, BAC is the only subtype without any invasive features. Obviously, an excellent prognosis can reasonably be expected for noninvasive BACs, and invasive features seen in adenocarcinoma are thought to be

prognostic. However, the relationship between the degree of pathologic invasion and prognosis has not yet been clarified.

In this retrospective study, we histopathologically graded the degree of invasion and explored the relationship between invasion and the prognosis of patients with adenocarcinoma, which might contribute to establishing the concept of "curable" lung cancer.

MATERIALS AND METHODS

Patients

For the 8-year period from January 1993 to December 2000, a total of 1045 pulmonary resections were performed for adenocarcinoma of the lung at the National Cancer Center Hospital, Tokyo. These comprised 60% of all resections for primary lung carcinomas performed during the same period (1738 resections). Among these 1045 adenocarcinomas, 384 tumors were ≤2.0 cm in diameter and located in the periphery of the lung parenchyma. Three cases with a past history of resection for other lesions and one case with preoperative treatment were excluded from this study. A total of 380 peripheral adenocarcinomas of ≤2.0 cm in diameter (36%) were studied to explore the relationship between the degree of invasive growth and prognosis. Clinicopathologic information was obtained by reviewing the medical chart in detail with regard to age, sex, mode of resection, recurrence, and survival. The surgical and postsurgical stages were determined according to the TNM system of the UICC.[26] The backgrounds of these 380 patients are summarized in Table 1. The patients ranged in age from 23 to 89 years with an average of 61.3 years. A total of 182 patients (48%) were male and 198 patients (52%) were female. Most of the patients (98%) underwent complete resection. As the mode of surgical resection, at least lobectomy was performed in 83%.

TABLE 1. Characteristics of Patients With Small Adenocarcinoma

Characteristic	Data
No. of patients	380
Age (years)	
Mean	61.3
Range	23–89
Gender	
Male	182 (48%)
Female	198 (52%)
Operative mode	
Pneumonectomy/lobectomy	314 (83%)
Segmentectomy/partial	66 (17%)
Lymph node dissection	
Mediastinohilar	227 (60%)
Hilar only/none	153 (40%)
Curability of surgery	
Complete	373 (98%)
Incomplete	7 (2%)
Histologic subtype by the WHO classification	
BAC	85 (22%)
Acinar	4 (1%)
Papillary	7 (2%)
Solid with mucin	27 (7%)
Mixed subtypes	257 (68%)
Pathologic stage	
IA	312 (82%)
IB	6 (1%)
IIA	21 (6%)
IIB	5 (1%)
IIIA	22 (6%)
IIIB/IV	14 (4%)

WHO, World Health Organization; BAC, bronchioloalveolar carcinoma.

Pathologic Evaluations

The resected specimens were routinely fixed with 10% formalin after lung inflation by intubation from the bronchus and embedded in paraffin. The entire nodules were blocked for histologic examination. Each of the specimens, including the largest cut surface of the tumor, was cut into 3-μm-thick sections. Sections of the tumor were stained by hematoxylin and eosin, periodic acid-Schiff, and elastica, and then examined by light microscopy. The histologic subtype was determined according to the WHO classification as BAC, acinar, papillary, solid with mucin, or adenocarcinoma with mixed subtypes. We strictly assigned a diagnosis of BAC for noninvasive tumors as defined by the WHO classification, where it is defined as "an adenocarcinoma with a pure bronchioloalveolar growth pattern and no evidence of stromal, vascular or pleural invasion." In this study, histopathological "invasion" was defined when the tumor cells were arranged in acinic/papillotubular structures or solid nests in a fibroblastic stroma, often accompanied by collagenization, and when the alveolar structures were no longer discernible (Fig. 1).[7,29] To categorize the degree of invasive growth in adenocarcinoma, four grades (0-3) were defined according to the location of the above-mentioned invasive features in adenocarcinoma lesions (Table 2). Lesions that were defined as having grade 0 invasion were consistent with BAC by the WHO classification. Typical histologic findings in each grade of invasion are shown in Figures 2 to 5. The following histopathologic findings were also evaluated in the same slides; tumor size (maximum tumor dimension), the size of the fibrotic focus within the tumor, degree of pleural involvement, vascular/lymphatic permeation, lymph node involvement, and pathologic stage. The size of the fibrotic focus was measured at the maximum dimension of the tumor after the fibrotic focus was diagnosed histologically in a low-power